Parametric optimization and comparative study of an organic Rankine cycle power plant for two-phase geothermal sources

Chaofan Chen[a,b], Francesco Witte[c], Ilja Tuschy[c], Olaf Kolditz[a,b], Haibing Shao[a,*]

[a] *Helmholtz Centre for Environmental Research-UFZ, Permoserstr. 15, Leipzig 04318, Germany*

[b] *Applied Environmental Systems Analysis, Dresden University of Technology, Dresden 01069, Germany*

[c] *Flensburg University of Applied Sciences, Flensburg 24943, Germany*

Abstract

For two-phase geothermal sources, Organic Rankine Cycle (ORC) based binary plant is often applied for power production. In this work, a network topology is designed with the open-source Thermal Engineering Systems in Python (TESPy) software to simulate the stationary operation of the ORC plant. With this topology, the performance of six different working fluids are compared. From the thermodynamic perspective, the gross and net power output are optimized respectively. Results show that R600 has the highest gross power output of 17.55 MW, while R245fa has the highest net power output of 12.93 MW. However, the turbine inlet temperatures for these two working fluids need to be designed at the upper theoretical limit. R245ca and R601a require the heat exchange rates of internal heat exchanger to be larger than 1.51 MW and 0.99 MW to satisfy the re-injection temperature limit, which are smaller than the R600 (6.7 MW) and R245fa (6.0 MW) cases. Besides, the working fluid with lower critical state is preferred for a geothermal source with smaller steam fraction to establish a stable ORC plant. The workflow for the ORC design and optimization in this work is generic, and can be further applied to thermo-economic investigation.

Keywords: Organic Rankine Cycle (ORC), Geothermal power plant,

*Corresponding author

Email addresses: chaofan.chen@ufz.de (Chaofan Chen), contact@witte.sh (Francesco Witte), ilja.tuschy@hs-flensburg.de (Ilja Tuschy), olaf.kolditz@ufz.de (Olaf Kolditz), haibing.shao@ufz.de (Haibing Shao)

Nomenclature

Roman letter

$\dot{m}$	mass flow rate ($\mathrm{kg\,s^{-1}}$)
$\dot{Q}$	heat power (W)
$\dot{W}$	power (W)
h	enthalpy ($\mathrm{J\,kg^{-1}}$)
p	pressure (bar)
pr	pressure ratio (-)
T	temperature (°C)
x	vapor mass fraction (-)
x_{IHE}	IHE sizing (-)

Greek letter

η	efficiency (-)

Operators

Δ	difference

Subscripts

1	hot side/topological location
2	cold side/topological location
af	air fan
am	ambient
ap	approach point

BEv	brine evaporator
el, m	electric, mechanical
fp	feed pump
gb	geothermal brine
geo	geothermal source
gs	geothermal steam
in	input
max	maximum
min	minimum
net	net
pp	pinch point
s	isentropic
t	turbine
th	thermal
u	upper terminal

Abbreviations

GWP	Global Warming Potential
IHE	Internal Heat Exchanger
ODP	Ozone-Depleting Potential
ORC	Organic Rankine Cycle
TESPy	Thermal Engineering Systems in Python

1. Introduction

Utilization of geothermal resource for power production is favored by the electricity grid due to its non-fluctuating feature in comparison to other types of renewable energy sources. In the geothermal industry, the number of Organic Rankine Cycle (ORC) based binary plants have been increasing steadily in recent years due to their superior performance in converting low- and medium-temperature heat sources to electrical power [1, 2]. Zarrouk and Moon [3] reported that the worldwide average conversion efficiency of geothermal power plant is around 12 %. For the binary power plants, this value is even lower. Therefore, the optimization of ORC design and the proper working fluid selection is critical for the economic feasibility of geothermal power projects. Currently, most of the designs and optimization of ORC plants were conducted based on pure liquid-phase geothermal resource with a temperature limit up to 200 °C [4, 5, 6, 7]. For a liquid geothermal source with temperature of 165 °C, El-Emam and Dincer [8] reported that the ORC energy conversion efficiency is 16.73 % in theory with the working fluid of isobutane (R600a). Fiaschi et al. [9] proposed an ORC plant for combined heat and power generation from medium-temperature liquid resource (up to 170 °C). In reality, although large proportion of the geothermal resources is liquid-dominated with a temperature range from 125 °C to 225 °C, there are often some steam fraction existing in the produced geothermal fluid [10, 11, 12]. The latent heat stored in the steam accounts for a considerable proportion of the total enthalpy. For example, in the Yangyi geothermal reservoir located in Tibet, China, the average wellhead temperature is 160 °C and steam mass fraction is about 10 % [13]. In this condition, the geothermal steam carries 2757.44 kJ/kg of energy, making the total enthalpy of two-phase geothermal fluid at 883.67 kJ/kg. With the 10 % additional steam, the geothermal fluid contains an extra of 208.20 kJ/kg enthalpy, or 30.82 % higher than its liquid-only form. Therefore, in order to achieve maximum power output from two-phase geothermal resource, the design and optimization workflow has to be adapted to fully utilize the energy stored in both geothermal brine and steam.

Technically, the two-phase geothermal ORC plants have two distinct features. First, latent heat in geothermal steam has to be fully extracted through evaporators and heat exchangers. Second, the re-injection temperature of geothermal fluid is usually limited by the saturation of silica or other minerals. For example, Grassiani [14] and Franco and Villani [15] reported in their studies that heat sink temperature has a lower limit of 70 °C in order to prevent silica scaling in the re-injection well. With heat sink temperature

constraint from the reservoir engineering side in consideration, Sun et al. [16] investigated the effects of evaporator pinch point temperature difference on the thermo-economic performance of the ORC plant. Franco and Vaccaro [17] proposed an integrated model including both the reservoir and power plant behavior. They also considered the re-injection temperature into the plant control strategy. However, their designs and optimizations were focused on the liquid-phase heat source, which cannot be directly applied to two-phase geothermal resource.

In order to achieve the maximum power output from an ORC plant, two issues need to be handled simultaneously, namely the ORC design and the working fluid selection [18, 19, 20]. First, the topological structure of the plant and the key parameters of components must be designed properly. In conventional ORC plants, the key parameters to achieve the maximum power output are turbine inlet pressure and temperature, along with the condenser outlet pressure and temperature [21, 22]. By varying the pinch point temperature difference, evaporation temperature and condensation temperature, Jankowski and Borsukiewicz [23] optimized the power output for utilizing low-temperature source of energy. In geothermal application, Vivian et al. [24] pointed out that the use of internal heat exchanger (IHE) may lead to a decrease in the heat recovery effectiveness when the geo-fluid has the lowest possible temperature. The use of an IHE is also referred as a technique called recuperation, the recuperative ORC [25] and the ORC with composition regulation [26] have been proposed to improve the cycle performance. Saleh et al. [27] and Dai et al. [28] also concluded that adding an IHE into an ORC system cannot increase the amount of gross power output, but only improve the thermal efficiency. Bina et al. [29] investigated the IHE influence from aspects of the energy, economic and environment, and concluded that systems with IHE installed are more efficient and environmental-friendly. Based on a 21 MW geothermal power plant in Turkey, Kahraman et al. [30] investigated the thermodynamic and thermoeconomic performances and analyzed the influence of ambient temperature on the power generation. Although this ORC plant is based on two-phase geothermal resources, their analysis was focused on the working fluid of R601 (n-Pentane) only.

Due to higher enthalpy stored in the two-phase geothermal sources, the second issue is the working fluid selection, which could lead to the significant variation in component size and the power output. Wang et al. [31] optimized a conventional ORC design with 13 working fluids, they concluded that the critical temperature of working fluid greatly affects the optimal evaporating pressure. Based on a liquid-phase geothermal resource at

96.85 °C, Aljundi [32] concluded that hexane has the best efficiency. They also found that the higher critical point temperature a working fluid has, the better thermal and exergetic efficiencies can be achieved in the ORC cycle. Focusing on sub-critical ORC system coupled with different heat sources, He et al. [33] pointed out that the working fluids with high liquid specific heat and low latent heat of evaporation should be selected, when the heat source temperature and mass flow rate are constant. Vivian et al. [24] also proposed a general framework to select working fluid and concluded that the distance between the fluid critical temperature and inlet temperature of the heat source plays a key role in predicting the optimum performance.

To the authors' best knowledge, although many researchers studied the thermodynamic or thermo-economic performance of ORC power plants for liquid-phase heat sources, the impact of different working fluids applied to two-phase geothermal ORC power plant has never been thoroughly investigated. In addition, a number of studies on the optimization of the ORC power plant were targeted for the maximum power output or thermal efficiency without the consideration of internal power consumption by feed pumps and air-cooler fans. Therefore, the highlight of this study is to present a design and optimization procedure, that is tailored for widely existing two-phase geothermal sources. The performance of six potential working fluids is compared and discussed. The optimization is further conducted for the maximum gross and net power output respectively, from thermodynamic perspective.

This paper is structured as follows: in section 2, the methodology of thermodynamic simulation and general optimization approach are introduced. This is followed by the description of an ORC plant design based on the conditions of ambient and two-phase geothermal sources in Tibet in section 3. Subsequently, the optimization objective and decision variables are clarified along with the optimization procedure (section 4). Then the parametric analysis and optimization results are presented in section 5. In section 6, the discussion is focused on the impact of IHE installation and geothermal steam mass fraction on the working fluid selection. Besides, the strategy of re-injection temperature control in geothermal ORC application is thoroughly discussed from the aspect of silica scaling in wellbore and tubes. At the last (in section 7), conclusions of this work are drawn and summarized.

2. Methodology

2.1. Thermodynamics modeling

For the thermodynamic modeling of ORC based geothermal power plant, the Thermal Engineering Systems in Python (TESPy) is employed in this study. TESPy is an open-source library that is capable of simulating stationary operation of thermal engineering applications. The library offers a variety of basic components like turbines, pumps, heat exchangers and piping components, which can be linked to form a power plant model. Each component applies basic balance equations for mass, energy and pressure as well as balance equations and constrains according to users' specification. Furthermore, a wide range of different working fluids is available by implementing the CoolProp library [34] as the thermodynamic property engine. For ORC plant relying on two-phase geothermal resource, properties of pure water is used in this work to represent the geothermal brine and steam [35].

To model an individual ORC plant, all components of the plant are connected in a network topology. TESPy automatically generates a set of non-linear equations based on this topology and applies the user-specified boundary conditions, e.g. isentropic efficiency of the turbine or pinch point temperature difference. The system of non-linear equations is solved using the multidimensional Newton-Raphson algorithm. The solver determines the values of the primary variables, i.e. mass flow, pressure, enthalpy and fluid mass fraction (in case of a liquid-gas mixture). Subsequently, every component parameter as well as the missing fluid properties, such as temperature, entropy or specific volume, can be determined from the primary variables [35].

2.2. Validation of the thermodynamics modeling

To validate TESPy models, the software repository includes a large variety of unit tests performed in the continuous integration, whenever changes are made to the source code. Among others, the tests refer to the governing equations available for connections and for components or even full models [35]. For instance, the model of a solar power plant has been built in EBSILON (industry standard in power plant simulation) and compared to the results obtained by TESPy. On top of that, the solar power plant model as well as the models of a refrigeration cycle and a super-critical CO2 power cycle have been validated in different work [36]. The validation results are available on GitHub: `https://github.com/fwitte/SEGS_exergy`, `https://github.com/fwitte/sCO2_exergy`, and `https://github.com/fwitte/`

`refrigeration_cycle_exergy`. Considering thorough validation of the software, no additional validation was specifically performed on the ORC system.

For the implemented governing equations of the components as well as the set of input parameters used in the geothermal ORC plant presented in this publication, please refer to the model reports in the Zenodo archive [37]. Furthermore, interested readers may refer to the online website for more information on the solver and other aspects of the software [38].

2.3. The ORC thermodynamic process analysis

To evaluate the performance of an ORC plant, the gross power $\dot{W}_{\mathrm{ORC}}$ generated by the thermodynamic cycle is an important value (Eq. (1)). Furthermore, the gross thermal efficiency of the plant can be used to describe the thermodynamic quality of the process, which is the ratio between gross power output and the heat input $\sum \dot{Q}_{\mathrm{in}}$. Due to the sign convention in TESPy, power produced by a turbine is always negative while power drawn by a pump or a fan will be positive. Therefore, the absolute value of the sum of power generated and consumed within the main cycle is considered here.

$$\dot{W}_{\mathrm{ORC}} = |\sum \dot{W}| \tag{1}$$

$$\eta_{\mathrm{th}} = \frac{\dot{W}_{\mathrm{ORC}}}{\sum \dot{Q}_{\mathrm{in}}} \tag{2}$$

However, the gross power does not take into account auxiliary power consumption, i.e. the power consumption of the condenser's air fans, and electrical conversion losses in generators as well as motors. Regarding the fan power consumption, much higher volumetric flow is required for cooling the working fluid compared to water-cooled systems as the air density is more than 800 times smaller than the density of liquid water, and heat capacity is smaller about 4 times (at 20 °C and 1.013 25 bar). Since the power drawn by the fan depends on the volumetric flow and the pressure increase, even a small pressure drop in the air stream through the condenser will result in a very high power demand. Details on the calculation of the fan power requirement can be found in the detailed model report [37]. Other auxiliary power requirements, e.g. by the control systems are neglected in this study. Finally, to obtain the net power output $\dot{W}_{\mathrm{net}}$ the electrical auxiliary power requirement is subtracted from the overall electrical power generated by

the cycle $\dot{W}_{\mathrm{el,ORC}}$ using Eq. (3). Net efficiency is then defined in Eq. (4) analogously to the thermal efficiency.

$$\dot{W}_{\mathrm{net}} = \dot{W}_{\mathrm{el,ORC}} - \dot{W}_{\mathrm{el,aux}} \tag{3}$$

$$\eta_{\mathrm{net}} = \frac{\dot{W}_{\mathrm{net}}}{\sum \dot{Q}_{\mathrm{in}}} \tag{4}$$

2.4. Numerical optimization

In this study, the optimization procedures are carried out on two different application scenarios, one with single parameter and the other with constrained multivariate optimization. As the numerical optimization is a widely covered research topic, this section only provides a concise overview on the optimization approaches selected in the current study. Interested readers might refer to e.g. Edgar and Himmelblau [39] and Ravindran et al. [40] for the detailed review on numerical optimization approaches available.

Generally, (constrained) optimization has the task to find the best possible solution to a problem regarding the objective $f(\vec{x})$ while respecting a set of equality $\vec{h}(\vec{x})$ and inequality constraints $\vec{g}(\vec{x})$. The advantage of using numerical optimization methods lies in the fact that the problem can be formulated as a black-box from the perspective of the optimization algorithm. Figure 1 illustrates the algorithms applied in this study. The objective and constraints (e.g. the re-injection temperature) are the result of the ORC power plant simulation given the value of the decision variables. By modifying the value of the each decision variable after solving the model, the algorithms will find the optimal solution to the objective while respecting the applied constraints without knowledge of the function inside of the black-box. Inside the black-box three basic tasks are performed, which are: (1) applying the values of the decision variables to the simulation model, (2) solving it and (3) calculating the objective value as well as the value of the constraints.

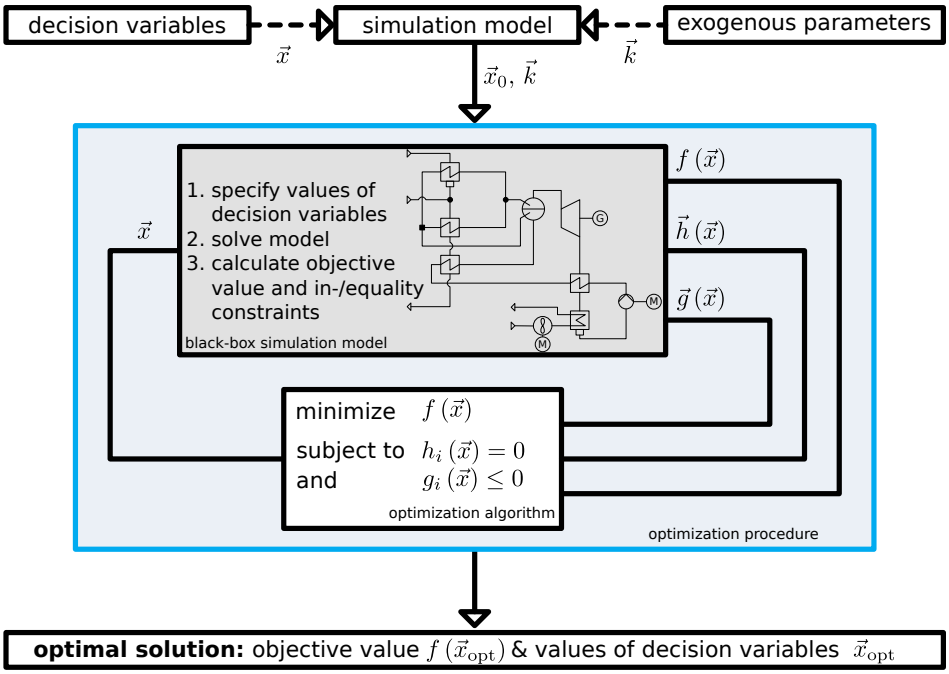

Figure 1: Abstract model of the optimization approach applied in this work.

For the single parameter optimization non-constrained problems, a robust and simple search algorithm needs to be applied. For example, the dichotomous or golden-section search as well as secant method or Newton's method. While the latter two approaches require the derivatives of functions (indirect methods), dichotomous and golden-section search work with function evaluation only (direct methods). The derivative (and second derivative for Newton's method) needs to be calculated numerically for the investigations in this study, therefore indirect search is inadequate in this case. As the golden-section search is considered the most efficient direct method and simple to implement [39, 41], it is chosen for this study.

Similar to the single parameter optimization, there are a variety of algorithms available for the constrained multivariate optimization. Again, due to the numerical nature of the black-box model, stochastic optimization methods are considered instead of the indirect method. The python implementation (pygmo) of the pagmo framework is therefore used in this work. It allows for easy integration into the source code and offers a large variety of algorithms covering exact as well as stochastic search methods. Depend-

ing on the particular optimization problem, an appropriate algorithm can be selected [42]. Due to having a constrained optimization problem, two global optimization methods from the framework are applicable: Extended Ant Colony Optimization [43] and Improved Harmony Search [44]. The improved harmony search algorithm showed high reliability and consistency in the results for the present study and was therefore applied.

3. System design

3.1. Background information

The heat source and ambient conditions of the ORC plant in this study are adapted based on the Yangyi geothermal site located in Tibet, China (cf. Wang et al. [13]). Major parameters are listed in Table 1. Since the production wells are located up in the mountains at 4800 m elevation and the ORC plant can only be constructed on the plain ground at 4650 m, connecting pipe lines have to be added to transport the geothermal fluid from the wellhead to the power plant. The heat loss along the pipe makes the temperatures of geothermal brine and steam to drop to 140 °C, which is lower than the value at wellhead as reported in the literature [13]. Hence, 140 °C is adopted as the heat source temperature for the power plant design, along with the annual average ambient temperature of 5 °C and absolute air pressure of 0.6 bar.

Table 1: Geothermal resource and ambient conditions

Item	Parameter	Symbol	Value	Unit
Geothermal resource	Steam temperature	T_{gs}	140	°C
	Steam mass flow rate	$\dot{m}_{gs}$	20	kg/s
	Brine temperature	T_{gb}	140	°C
	Brine mass flow rate	$\dot{m}_{gb}$	180	kg/s
	Steam mass fraction	x	0.1	-
	Brine/steam pressure	p_{geo}	3.615	bar
Ambient condition	Average temperature	T_{am}	5	°C
	Average pressure	p_{am}	0.6	bar

3.2. Topological structure of the plant

The flow diagram of the ORC power plant for two-phase geothermal resource is shown in Fig. 2(a), with the T-s diagram in Fig. 2(b) and the preheater's and evaporators' T-Q diagram shown in Fig. 2(c). The following

components are included in the ORC plant: a preheater, two evaporators (one using the geothermal steam and the other using the brine), a drum for separating the saturated liquid from the saturated steam, a turbine connected to a generator, an internal heat exchanger (optional), an air-cooled condenser with air fans and a feed pump for circulating the working fluid.

In this system design, latent heat in the geothermal steam is fully exchanged in the geo-steam evaporator, where the geothermal steam is condensed to the saturated liquid state. Subsequently, the condensed geo-fluid is mixed with the geothermal brine before entering the geo-brine evaporator to further provide heat. The remaining sensible heat stored in the geothermal brine coming out of the geo-steam evaporator is extracted through a preheater before being re-injected into the reservoir. The drum separates the saturated liquid from the saturated gas phase of the working fluid. The saturated liquid phase is routed through both evaporators in parallel and partially evaporated. The saturated gas phase powers the turbine. The exhausting heat can be recovered (optionally) by an IHE, preheating the liquid working fluid. Due to the lack of feasible water cooling options at the Yangyi site, an air-cooled condenser is implemented to condensate the working fluid. Thus, air fans are required. Finally, the saturated liquid-phase working fluid is pressurized by the feed pump. Both air fans and the feed pump are driven by electrical motors.

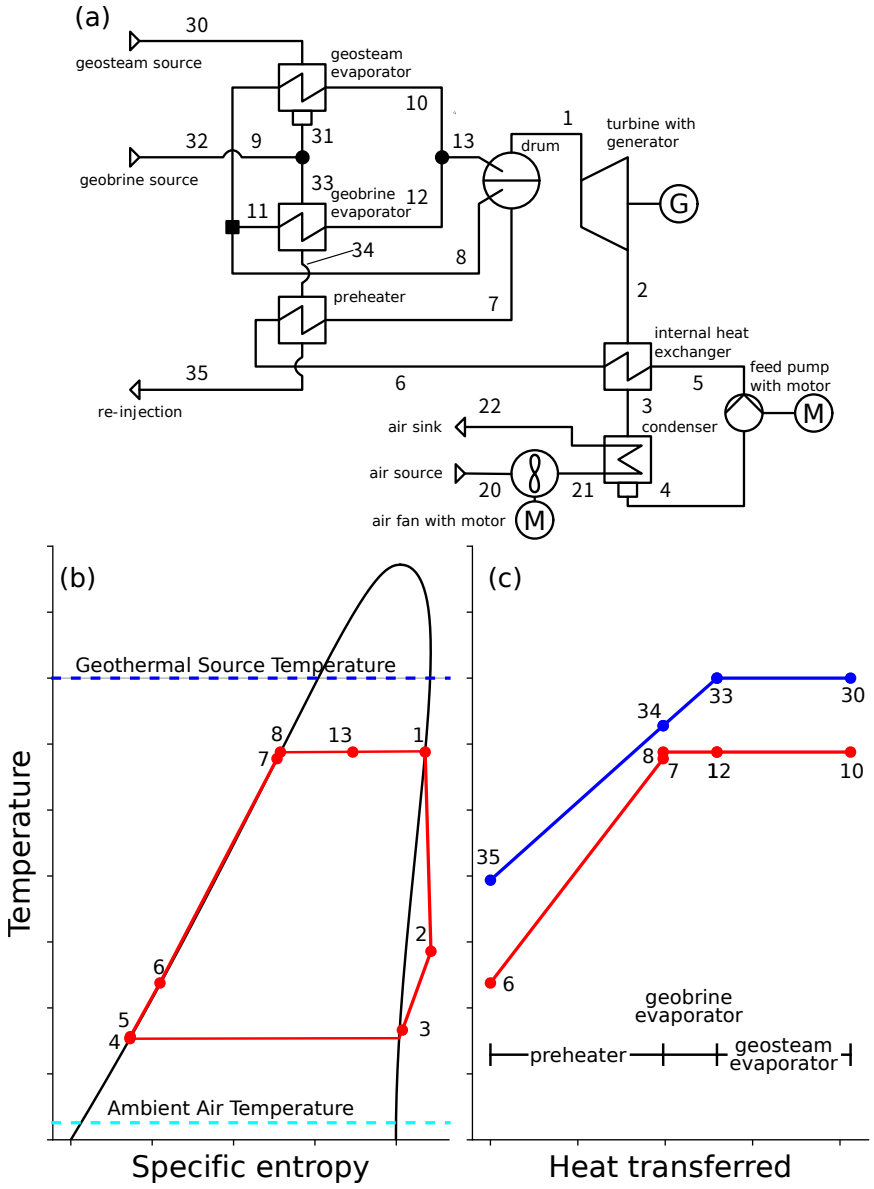

Figure 2: The two-phase geothermal ORC plant design: (a) Schematic and major components layout, (b) the respective Ts-diagram of the ORC, and (c) the T-Q diagram of the preheater and evaporators.

The T-Q diagram of the preheater and evaporator indicates that the potential for overheating the working fluid after evaporation is comparably low (about 20 °C in the example shown). Although a higher turbine inlet tem-

perature is thermodynamically favorable, overheating the fluid does require an additional component. Given the low overheating potential, the effort of building a super-heater which uses the condensing geo-steam for overheating is unreasonably high. Therefore, this work does not employ an additional heat exchanger for overheating the working fluid. This also restricts the choice of the working fluid to dry or isentropic fluids [45]. Nine potential working fluids are initially selected in this work for the design: R245fa, R600 (n-butane), R245ca, R123, R113, R11, R141B, R601a (Isopentane) and R601 (n-Pentane). For these fluids, the gradient of the dew line is positive as shown in Fig. 3. The critical state of each potential working fluid are listed in Table 2. When looking into the environmental property of nine potential working fluid, R113 and R11 are firstly excluded because of the high GWP and ODP values. As for the toxicity and environmental property, R123 is not suitable for the power plant due to its high level of toxicity, while R245fa is still considered for the comparison between R600 as they have a similar critical state. Therefore, after preliminary screening, the discussed potential working fluids in following results are focused on R245fa, R600 (n-butane), R245ca, R141B, R601a (Isopentane) and R601 (n-Pentane).

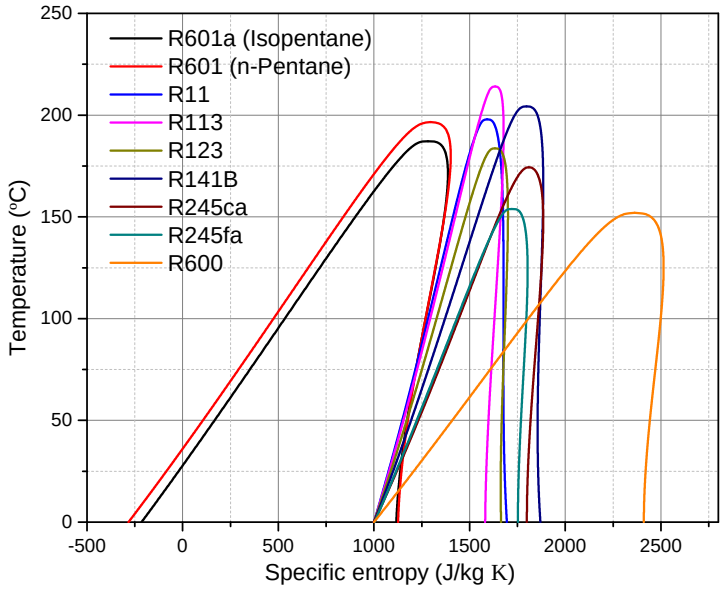

Figure 3: Non-negative slope of saturated vapor curve for nine selected working fluids

Table 2: Main thermodynamic, safety and environmental properties of nine potential working fluids

Working fluid	Critical temperature (°C)	Critical pressure (bar)	GWP (100 years)	ODP	ASHRAE 34 Safety Group
R245ca	174.42	39.41	716	0	-
R601a (Isopentane)	187.20	33.78	4 ± 2	0	A3
R601 (n-Pentane)	196.55	33.68	4 ± 2	0	A3
R123	183.68	36.62	79	0.02	B1
R113	214.06	33.92	5,820	1.0	A1
R141B	204.35	42.12	725	0.12	A2
R11	197.91	44.04	4660	1.0	A1
R245fa	153.86	36.51	858	0	B1
R600	151.98	37.96	4.0-6.5	0	A3

3.3. Design parameters of the plant

The fixed design parameters of the ORC plant are summarized and listed in Table 3. All parameter assumptions are derived from industrial standard values for the corresponding components.

A low pinch point temperature is always favorable, as thermodynamic losses of heat transfer will be lower and evaporation temperature will be higher. However, lowering pinch point requires more heat exchange surface and thus increasing the initial investment as well as the draft side loss [46]. Therefore, a pinch point temperature difference of 8 °C is selected in this study. Analogous to the pinch point specification, the upper terminal temperature difference of the condenser determines the thermodynamic losses and its size. As the working fluid is condensed by ambient air, the heat transfer coefficient is expected to be lower than in the geothermal brine evaporator. Therefore, a slightly higher terminal temperature difference value of 10 °C is chosen. The isentropic efficiency of the turbine is assumed to be 90 %, with lower values for the feed pump (75 %) and the air fan (60 %). The conversion losses of all motors and generators of the turbo-machinery are assumed to be 3 %.

Pressure losses in the heat exchangers are taken into account in the following way: Condensation in the geo-steam evaporator and main condenser does not inflict pressure losses, therefore the pressure ratio pr is equal to one. The air condenser pressure loss is assumed to be 0.5 %, while internal pressure losses in the IHE, the preheater and the geo-brine evaporator hot side are at 2 %. For the evaporating working fluid in both evaporators it

Table 3: Design parameters of the ORC system

Location	Parameter	Symbol	Value	Unit
Turbine	Isentropic efficiency	$\eta_{\mathrm{s,t}}$	90	%
Feed pump	Isentropic efficiency	$\eta_{\mathrm{s,fp}}$	75	%
Air fan	Isentropic efficiency	$\eta_{\mathrm{s,af}}$	60	%
Main condenser	Upper terminal temperature difference	$\Delta T_{\mathrm{t,u}}$	10	°C
	Pressure ratio on hot side	pr_1	1	-
	Pressure ratio on cold side	pr_2	0.995	-
Geo-steam evaporator	Pressure ratio on hot side	pr_1	1	-
	Pressure ratio on cold side	pr_2	1	-
Geo-brine evaporator	Pinch point temperature difference	ΔT_{pp}	8	°C
	Pressure ratio on hot side	pr_1	0.98	-
	Pressure ratio on cold side	pr_2	1	-
IHE & preheater	Pressure ratio on hot side	pr_1	0.98	-
	Pressure ratio on cold side	pr_2	0.98	-
Preheater outlet	Approach point temperature difference	ΔT_{ap}	2	°C
Generator	Efficiency	$\eta_{\mathrm{el,m}}$	97	%
Motors	Efficiency	$\eta_{\mathrm{el,m}}$	97	%

is assumed that the evaporation is in natural circulation, thus inflicting no pressure losses.

4. System optimization

4.1. Objective and decision variables

Similar to a combined steam cycle power plant, optimization of efficiency is not appropriate, but instead the total power generation [47]. The optimization of heat recovery steam generators in combined cycle power plants is a well known topic in thermal engineering, e.g. Bejan et al. [48], Roosen et al. [49], Silveira and Tuna [50], Valero et al. [51]. Therefore, the optimization in this study was conducted from the thermodynamic perspective for the maximum gross ($\dot{W}_{\mathrm{ORC}}$) and net ($\dot{W}_{\mathrm{net}}$) power output, respectively.

A set of parameters do not have an obvious optimum regarding the plant's performance. Therefore, they are subject to the designer's choice

(decision variables), including the turbine inlet temperature, the IHE size, and the change of air temperature in the condenser related to the condensing temperature. The decision variables are listed with their corresponding minimum and maximum boundaries in Table 4.

Table 4: Minimum and maximum values of the parameters for the optimization

Parameter	Symbol	Minimum	Maximum	Unit
Turbine inlet temperature	T_1	50	132	°C
IHE sizing	x_{IHE}	0	1	-
Air temperature difference	ΔT_{air}	5	25	°C

The upper limit of the turbine inlet temperature is constrained by the pinch point temperature difference (ΔT_{pp}) and the saturation temperature of the geothermal brine as calculated by Eq. (5). Its lower limit is determined by the fact that the outlet pressure of the turbine must be lower than its inlet pressure. Therefore, the temperature at the inlet of the turbine must be higher than the maximum possible outlet temperature, which can be determined starting from the air temperature with Eq. (6).

$$T_{1,\mathrm{max}} = T_{32} - \Delta T_{\mathrm{pp}} \tag{5}$$

$$T_{1,\mathrm{min}} = T_{20} + \Delta T_{\mathrm{t,u,cond}} + \Delta T_{\mathrm{air,max}} + \Delta T_{\mathrm{safety}} \tag{6}$$

The IHE size of is applied using a user defined equation in the thermodynamic model (Eq. (7)), in which x_{IHE} reflects the ratio of heat exchanged in the IHE to its maximum possible value.

$$0 = h_3 - h_2 - x_{\mathrm{IHE}} \cdot (h_3 - h\,(p_2, T_5 + \Delta T_{\mathrm{t,u,min}})) \tag{7}$$

The upper limit of the heat exchange ratio is $x_{\mathrm{IHE}} = 1$, meaning that the maximum possible heat is exchanged as the outlet temperature at the gas side of the IHE is at its minimum possible value (cold side inlet temperature plus upper terminal temperature difference). In this study, $\Delta T_{\mathrm{t,u,min}}$ is set at 2 °C. In the case without IHE installed, $x_{\mathrm{IHE}} = 0$ and h_3 must be equal to h_2.

Finally, the last parameter subject to the optimization is the change of air temperature difference in the condenser ΔT_{air}, which is applied to the model using Eq. (8). As described, its value determines the air flow through

the condenser (but not the heat transferred) and subsequently the total electrical power drawn by the motor of the air fan.

$$0 = T_{22} - T_{21} - \Delta T_{\text{air}} \tag{8}$$

Here the temperature constraints can be chosen freely, and are set to 5 °C as the lower and 25 °C as the upper limit.

In addition to the decision parameters listed in Table 4, the re-injection temperature also has lower limit for the ORC application in hydro-thermal geothermal systems. The rejection temperature should be high enough to avoid silica over-saturation in geo-brine, which could lead to silica scaling and serious fouling problems in recovery heat exchangers, and in mineral deposition in pipes, valves and re-injection wellbores [52, 53, 54]. However, too high rejection temperatures can make the exploitation of such a system unprofitable. In that case, the lower limit value of re-injection temperature in this study is selected at 70 °C, the same as reported by Grassiani [14], Franco and Villani [15].

4.2. Optimization procedure

In order to achieve the optimal design of each potential working fluid, the optimization is conducted in the following four steps to calculate the gross and net power output, respectively.

In the first step, the ORC cycle is designed with no IHE installed. That means, the heat transferred on the IHE is set to 0 W and no pressure losses are inflicted. Also, the air temperature difference in the condenser is assumed to be fixed at 15 °C. In the ORC design, due to the working fluid being kept in the saturated vapor state before entering the turbine, the status of working fluid at the inlet of turbine can be regulated by its temperature only. The influence is investigated for all the potential working fluids, and the results are analyzed in section 5.1.

With the aforementioned configuration, the maximum gross power output value can be found for each working fluid. In the second step, the gross power output is optimized by using golden-section search method with a single parameter of the turbine inlet temperature. For the optimal ORC design without IHE installed, the detailed thermodynamic parameters at key connections are summarized and listed in section 5.2.

Since most geothermal plants have a lower limit on the re-injection temperature (e.g. 70 °C in this case), an IHE has to be installed in the ORC plant for some working fluids. Therefore, in the third step, the impact of IHE size on re-injection temperature is investigated in section 5.3, with the

turbine inlet temperature value fixed at the optimum point as in the second step. Besides, the impact of IHE is reflected in the net power output as well.

Looking into the net power output, the air temperature increase in the condenser determines the air mass flow rate of the fan and its power consumption. Therefore, its influence is investigated in section 5.4. Subsequently in the fourth step, the net power output is optimized with the three decision variables, i.e. the turbine inlet temperature, condenser air temperature increase and the IHE size. This leads to section 5.5, where the maximum net power output and optimal ORC design for the two-phase geothermal sources is finally obtained.

5. Results

5.1. Influence of the turbine inlet temperature

When no IHE is installed, the heat exchange rate is set to 0 W and there is no IHE pressure losses. Besides, the air temperature difference in the condenser is kept at 15 °C when investigating the influence of turbine inlet temperature.

For the six working fluids, when the turbine inlet temperature is changing within the theoretical range (cf. section 4.1), the gross power output and re-injection temperature respond accordingly. Among all the six fluids, four of them show similar trend (see Fig. 4(a)-(f)). With the ascending turbine inlet temperature, the gross power output increases first and then decreases after reaching a peak. In comparison, R245fa and R600 show different behaviors, the gross power output continuously increase along with the ascending turbine inlet temperature.

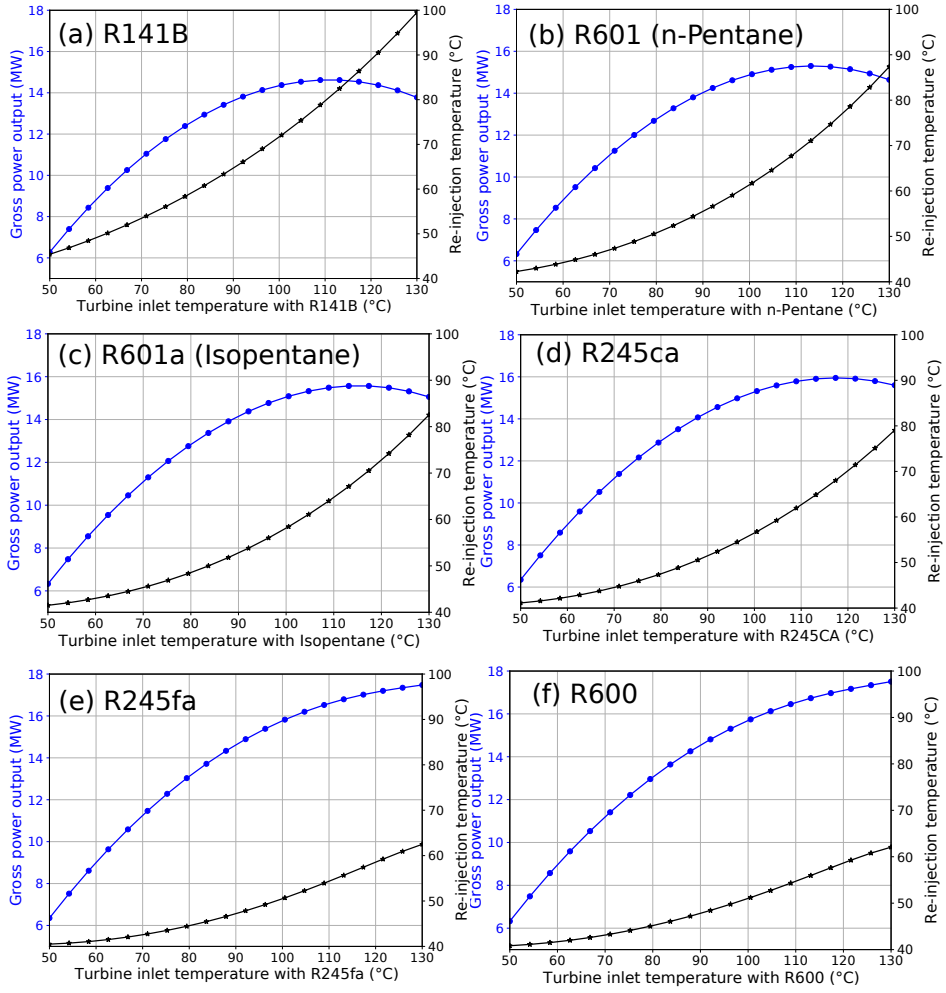

Figure 4: Gross power output and re-injection temperature under different turbine inlet temperatures with the working fluid of (a) R141B (b) R601 (n-Pentane) (c) R601a (Isopentane) (d) R245ca (e) R245fa (f) R600.

For the re-injection temperature from the ORC plant, all the six working fluids show the same change trend, continuously increasing as the turbine inlet temperature increases. Due to the fixed pinch point temperature difference (ΔT_{pp}), a higher turbine inlet temperature will decrease the mass flow rate of the working fluid, and increase the re-injection temperature. For example, the mass flow rate of R245ca decreases from 582.52 kg/s

to 344.42 kg/s, when the turbine inlet temperature changes from 50 °C to 130 °C. This leads to an increase of 37.92 °C for the re-injection temperature from the ORC plant.

It is worth noting that R600 and R245fa produce much higher gross power output, both approaching 18 MW. This is because the two fluids result in a very low re-injection temperature, ranging from 40 °C to 60 °C as shown in Fig. 4(e) and Fig. 4(f). The heat exploitation from the geothermal source is therefore much higher. Since the thermal efficiency is at a similar level for all fluids, the total power output is higher for R600 and R245fa.

5.2. The optimal design without an IHE

Based on the analysis above, the optimal turbine inlet temperature for the maximum gross power output without an IHE can be obtained by applying the golden section search algorithm. The detailed results of the optimal design is presented in Table 5, listing all state parameters of each working fluid at key connecting points of the plant. These parameters include the temperature at the turbine inlet, the turbine outlet, the re-injection point, along with the power output, and the thermal efficiency values. For R600 and R245fa, the turbine inlet temperature is at 131 °C that is lower than the theoretical upper limit listed in Table 4. This is due to the nature of the golden section search, as it will not exactly find a value located at the edge of the search range.

Table 5: The optimal design for the maximum gross power output without IHE installed.

Item	R245ca	R601a	R601	R141B	R245fa	R600
T_1 (°C)	117.58	115.29	113.59	111.09	131.00	131.00
T_2 (°C)	56.75	63.12	61.45	41.93	50.02	50.31
p_2 (bar)	1.24	1.12	0.84	0.97	1.82	2.89
T_{35} (°C)	68.19	68.81	71.41	80.66	62.81	62.31
Q_{BEv} (MW)	12.31	14.26	15.69	17.82	0.86	0.86
$\dot{W}_{\mathrm{ORC}}$ (MW)	15.95	15.58	15.30	14.63	17.51	17.55
$\dot{W}_{\mathrm{net}}$ (MW)	11.44	11.09	10.92	10.59	12.79	12.79
η_{th} (%)	15.40	15.12	15.17	15.71	16.20	16.17
η_{net} (%)	11.05	10.76	10.82	11.38	11.84	11.79

It can be seen from Table 5, the optimal turbine inlet temperature varies from 111.09 °C with R141B to 117.58 °C with R245ca. The re-injection temperatures in the optimal design for R601 (n-Pentane) and R141B are all higher than 70 °C. R601 (n-Pentane) have a higher gross power output, both reaching 15.30 MW. R141B has the gross power output of 14.63 MW. With

R245ca and R601a (Isopentane), the gross output is found to be 15.95 MW and 15.58 MW respectively, which are higher than the other two working fluids mentioned above. As for the working fluid of R600 and R245fa, the thermal conversion efficiency and power output are both higher than the other four fluids. However, the re-injection temperature with these two fluids is far lower than the limit of 70 °C.

When looking into the net power output, R601 (n-Pentane) is 0.33 MW higher than R141B, which is less than the gross power difference (0.67 MW). This indicates that the auxiliary power consumption is 0.34 MW lower for R141B, leading to a higher thermal efficiency of 15.71 %. For R245ca and R601a (Isopentane), because of the high gross power output, their net power outputs are both higher than 12 MW. Despite of the second largest amount of gross power output for the R601a (Isopentane) (15.58 MW), their gross and net thermal efficiency is the lowest (15.12 % and 10.76 %).

In the optimal design of R245ca and R601a (Isopentane) for the maximum gross power output, the re-injection temperatures are both lower than 70 °C. The working fluid temperature before entering the condenser is 56.75 °C for R245ca and 63.12 °C for R601a (Isopentane). The values are far away from saturation temperature of the working fluid, which is at 30 °C in the design. This implies that a large proportion of the heat stored in the working fluid steam leaving the turbine needs to be released to the environment. This results in a large size of the condenser and low system efficiency. To improve the cycle performance and efficiency, an IHE can be installed to recover part of the heat from the working fluid out of the turbine, and thus reduce the condenser size. Additional benefit of the IHE is an elevated re-injection temperature, as well as improved net power output due to the lower air mass flow required for cooling. For R245fa and R600, one of the distinct features is the heat exchange rate of brine evaporator (Q_{BEv}) are quite smaller compared to another four working fluids. This is because the optimized turbine inlet temperature (131 °C) is very close to the critical temperature of R245fa (158.36 °C) and R600 (151.98 °C), resulting in a relatively small evaporation heat required by the working fluid in geo-brine and geo-steam evaporators. Because the assumption that geo-steam evaporator exchanges all latent heat from the geothermal steam source, most of the evaporation heat required by the working fluid can be provided by the geo-steam evaporator. Therefore, the heat exchange rate of geo-brine evaporator accounts for a very small ratio as listed in Table 5. Besides, due to the low re-injection temperature of 62.81 °C and 62.31 °C, a large IHE has to be installed to avoid silica scaling.

5.3. Influence of the internal heat exchanger

With the re-injection temperature limit of 70 °C, four (R245ca, R601a (Isopentane), R245fa and R600) out of the six working fluids selected in this work cannot be directly applied to silica bearing geothermal fluid without the installation of an IHE. The pressure loss of the IHE component is represented by the pressure ratio at the hot and cold sides. The ratio at hot and cold sides are both set to be 0.98.

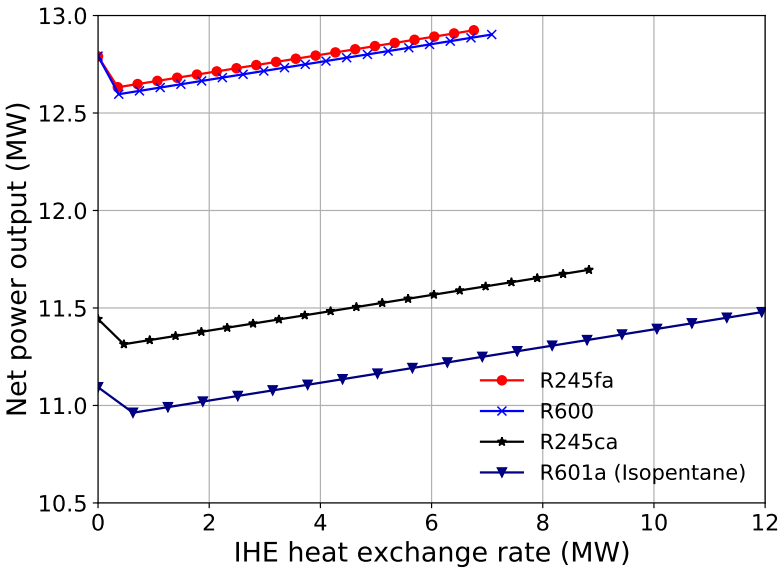

Figure 5: Net power output under different heat exchange rates of the IHE in the ORC. The turbine inlet temperature is fixed at 117.58 °C for R245ca, 115.29 °C for R601a (Isopentane) and 131 °C for R245fa and R600.

For R245ca, R601a (Isopentane), R245fa and R600, the net power output and re-injection temperature are compared, when the x_{IHE} value ranges from 0 to 1. It is noticed that with the same x_{IHE} value, the amount of heat exchanged with different working fluid can vary dramatically. For example, when $x_{\mathrm{IHE}} = 1$, the IHE heat exchange rate is 8.83 MW for R245ca, 11.93 MW for R601a (Isopentane), 6.76 MW for R245fa, and 7.08 MW for R600, respectively. Therefore, Figure 5 and Figure 6 depict the influence of IHE using the heat exchange rate as the x-axis. In these two figures, the upper limit of the IHE heat exchange rate also indicates the maximum recoverable heat from the working fluid vapor leaving the turbine.

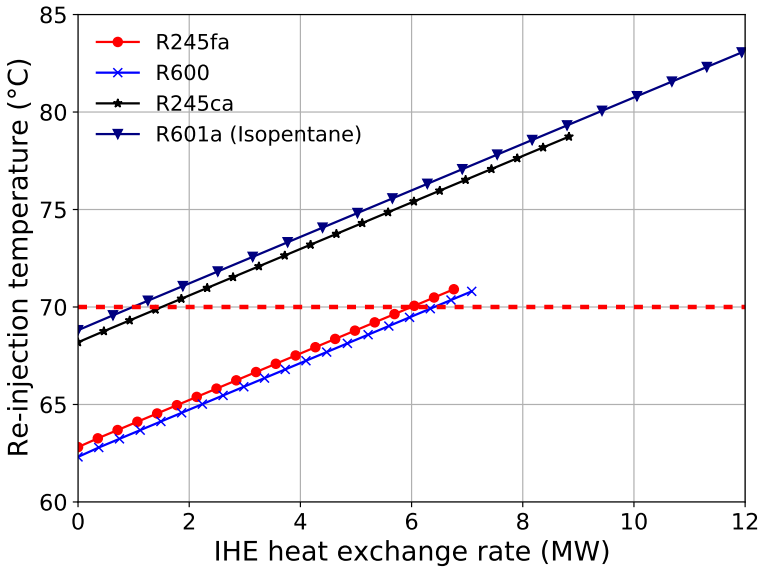

Figure 6: Re-injection temperature under different heat exchange rates of the IHE in the ORC. The turbine inlet temperature is fixed at 117.58 °C for R245ca, 115.29 °C for R601a (Isopentane) and 131 °C for R245fa and R600.

As illustrated in these two figures, the net power output and re-injection temperature are both linearly dependent on the growing size of IHE. In Fig. 5, a slight drop in net power output can be observed as soon as the IHE is introduced. That is caused by the pressure loss in the IHE component when it is included ($x > 0$).

With the clear trend presented in Fig. 6, it is straightforward to find the proper IHE size that makes the re-injection temperature higher than 70 °C (the red dash line). For R600 and R245fa, the heat exchange rate of the IHE has to be larger than 6.7 MW and 6.0 MW. In contrast, the required IHE capacities for both R245ca and R601a (Isopentane) are smaller than 2 MW, which means the smaller IHE size and more saving initial investment.

Exemplary, the T-s diagrams of the R245ca and R600 based ORC plants are illustrated in Fig. 7, with the maximum size IHE ($x_{\mathrm{IHE}} = 1$) installed in the system.

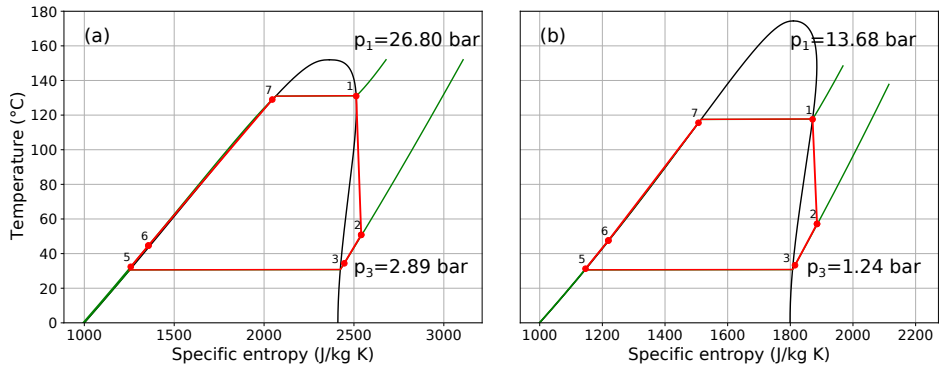

Figure 7: T-s diagrams of the ORC plant with working fluids (a) R600 and (b) R245ca, when the largest IHE ($x_{\mathrm{IHE}} = 1$) is installed. The turbine inlet temperature is at the optimal value from Table 5.

The installation of the IHE and the selection of its size essentially affects the distance between the point #3 and saturation as well as the point #6 from the point #5 in Fig. 7. When the maximum IHE is installed, the working fluid state before entering the condenser (point #3) can be kept very close to the corresponding saturation point. In that case, the heat after point #2 can be mostly recovered, resulting in a relieved thermal load on the condenser, which effectively reduce the required mass flow rate with a given air temperature difference. This leads to the benefit of a lower electricity consumption of the air fan and an increase of the net power output. In addition to that, the re-injection temperature is elevated as well.

5.4. Influence of the condensing temperature

In an ORC plant, the condensing temperature also has a significant influence on the net power output. The value is determined by the cooling air temperature difference in the design as listed in Table 4. In order to directly reflect the influence of condensing temperature, the cooling air temperature difference in Table 4 is converted into the condenser outlet temperature, which ranges from 20.66 °C to 45.66 °C considering the isentropic efficiency of the air fan in the condenser (60 %). The influence for the six working fluids is presented in Fig. 8. For all the working fluids, the turbine inlet temperature is fixed at 114 °C. The IHE is designed at the maximum size.

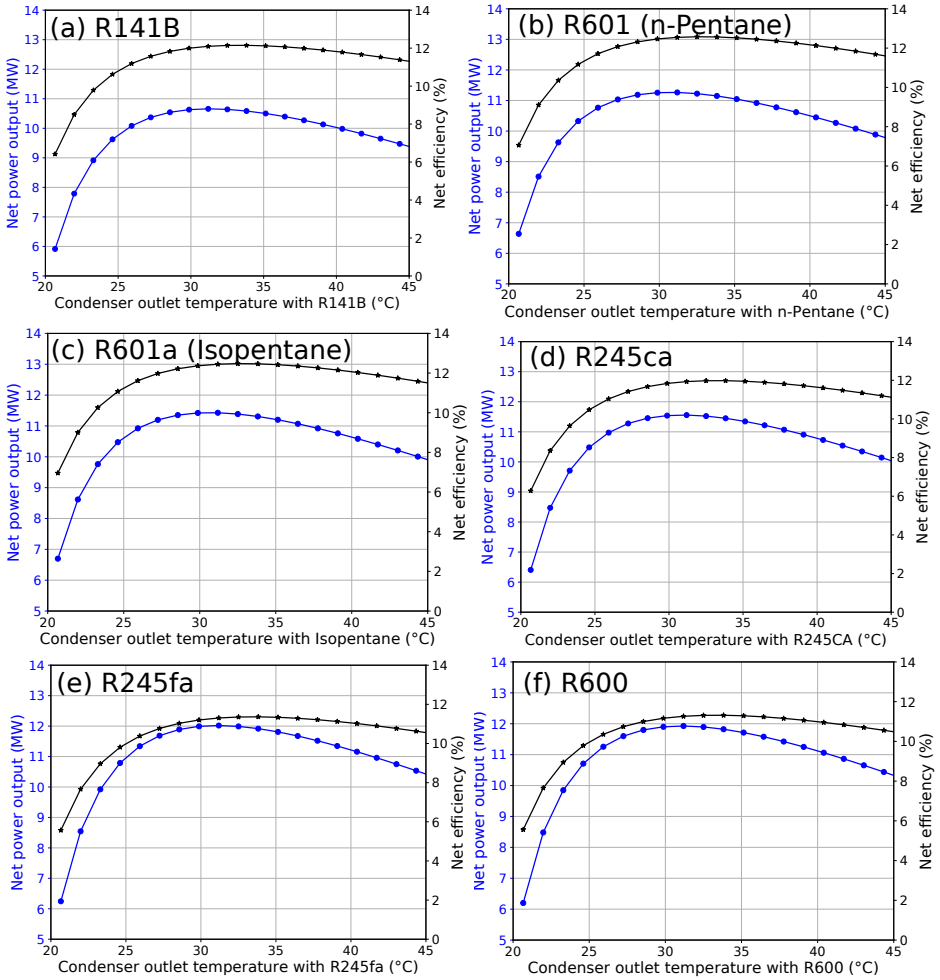

Figure 8: Net power output and net efficiency for the six working fluids within the range of condenser outlet temperature between 20 °C and 45 °C. The maximum possible IHE ($x_{\mathrm{IHE}} = 1$) is installed and the turbine inlet temperature is fixed at 114 °C.

For all the six working fluids, when the designed air temperature difference in the condenser is increased, the temperature at the outlet of the condenser is increased as well due to the fixed upper terminal temperature difference. However, the mass flow rate of working fluid remains unchanged, because the inlet temperature of the turbine is fixed. Therefore, the gross power output and thermal load of the condenser is reduced, leading to a

low mass flow rate of the cooling air and electric power consumed by the air fan. When the condenser outlet temperature is largely increased, the gross power output will drop significantly due to the decreased change of pressure in the turbine, resulting in a low net power output despite of the savings from the air fan. This explains the net power output increases first and decreases after reaching a peak, along with the condenser outlet temperature increasing.

Different from the turbine inlet temperature influence on the gross power output, R245fa and R600 presented in Fig. 8 clearly have the optimal value of the condenser outlet temperature for the maximum net power output. For R245fa, when the condenser outlet temperature increases from 20.66 °C to 45.66 °C, it results in the gross power output to drop from 19.72 MW to 13.01 MW. Meanwhile, the electricity consumption by the condenser air fan decreases more significantly, from 12.68 MW to 1.95 MW. Thus, the net power output increases from 6.25 MW to 10.31 MW.

When the IHE is installed with the maximum size, the net efficiency changes in a similar trend as the net power output. It increases first and then decreases after reaching a peak. The highest value occurs in R601 (n-Pentane) plant when the turbine inlet temperature is fixed at 114 °C, reaching more than 13 %. In addition, as stated in section 4.1, the respective optima of net power output and net efficiency are at different design conditions.

5.5. Multivariate optimization of the net power output

By combining the influence analysis above, the ORC design can be optimized for the maximum net power output by using Pygmo library (see section 2.4). In this section, different turbine inlet temperatures, IHE sizes and condenser outlet temperatures are simultaneously changed for the maximum net power output. The maximum net power output values of the six working fluids are presented in Fig. 9. And the optimal decision variables for each working fluid are summarized and listed in Table 6. The data presented have been calculated based on 10 individuals per population, each evolved 30 times.

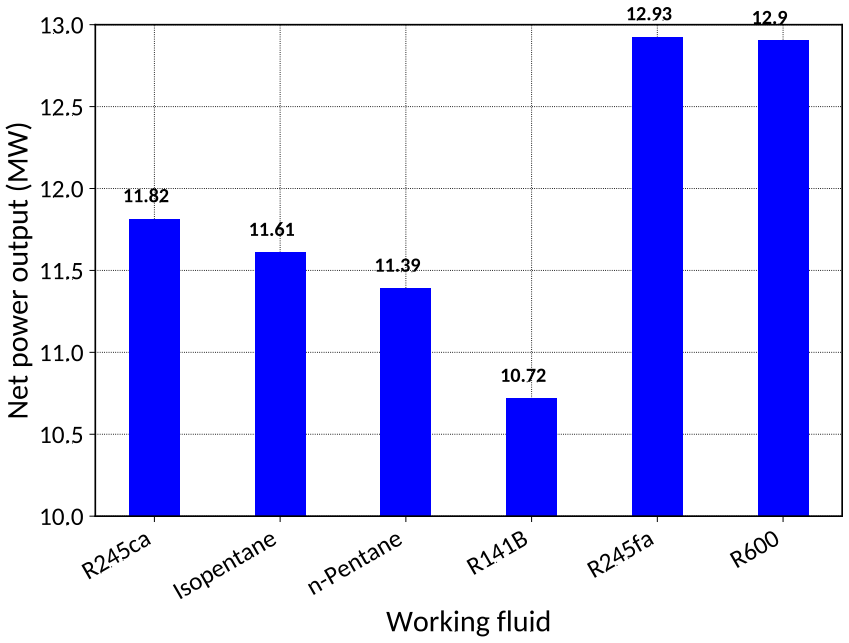

Figure 9: The maximum net power output of the six working fluids

Table 6: The optimal design for the maximum net power output

Working fluid	$\dot{W}_{\text{net}}$ (MW)	T_1 (°C)	ΔT_{air} (°C)	x_{IHE} (-)	T_{35} (°C)
R245ca	11.82	125.12	15.21	1	85.24
R601a (Isopentane)	11.61	123.01	14.92	1	90.02
R601 (n-Pentane)	11.39	121.46	14.98	1	91.38
R141B	10.72	119.29	15.57	1	91.70
R245fa	12.93	131.00	15.43	1	71.17
R600	12.90	131.00	15.38	1	71.03

It is found that the highest net power output predicted by the optimization procedure reaches 12.93 MW with R245fa. The second highest value is 12.91 MW with R600, and it is followed by R245ca at 11.82 MW. The lowest output among all working fluids is found to be with R141B at 10.72 MW. Although the net power output of R245ca plant is 1.11 MW less than R245fa and 1.08 MW less than R600, R245ca is the preferred working fluid in a stable plant design, as the turbine inlet temperature of R245fa and R600 both needs to be designed at their theoretical upper boundaries.

As expected, the IHE is always designed at the largest size for all the six working fluids to have the maximum net power output as listed in Table 6. Due to the maximum IHE installed, the re-injection temperature can be kept higher than 70 °C for all the six working fluids. The low values in re-injection temperature for R245fa and R600 also explain the gap in net power output to the other fluids.

6. Discussion

6.1. IHE installation

For geothermal power plants, the IHE controls not only the re-injection temperature, but also the initial investment. Among all types of working fluids, there are three typical categories in how to determine the IHE size.

In the first category, the re-injection temperature limit can be satisfied even without the installation of IHE. Since the re-injection temperature is higher than 70 °C, two working fluids, i.e. R141B and R601 (n-Pentane), do not require an IHE to be included in the ORC plant in this study. However, the gross power output of these fluids is also low, ranging from 14.63 MW to 15.30 MW. They are about 16.64 % to 17.44 % lower than the highest gross output of 17.55 MW with R600. For designers, the choice of this type of working fluids means that the investment on the IHE can be saved with the expense of low gross power output.

In the second category, a small IHE has to be installed in order to satisfy the constraint in re-injection temperature. In this study, R245ca and R601a (Isopentane) belong to this category. When the turbine inlet temperature is fixed at its optimal value, the re-injection temperature is 68.19 °C for R245ca and 68.81 °C for R601a (Isopentane) without an IHE installed in the plant. In that case, a small IHE size can make the re-injection temperature higher than 70 °C. The required IHE heat exchange rate is 0.99 MW for R601a (Isopentane) and 1.51 MW for R245ca. For each working fluid, the lower the turbine inlet temperature, the larger IHE is required.

The third special category includes R245fa and R600 in this study. Both fluids have very large gross and net power output values. The special characteristics of these two fluids is that the required IHE size varies dramatically with the change in turbine inlet temperature. When the re-injection temperature is fixed at 70 °C, Figure 10 depicts the required IHE size in response to the varying turbine inlet temperature. For R245fa, if the geothermal resources is degrading over the years and the turbine inlet temperature drops from 131 °C to 126 °C, the required IHE size has to be increased from 6.0 MW to 7.8 MW, which is nearly a 30 % increase. From engineering point of view,

this means the plant needs to retrofit additionally an IHE device after couple of years operation.

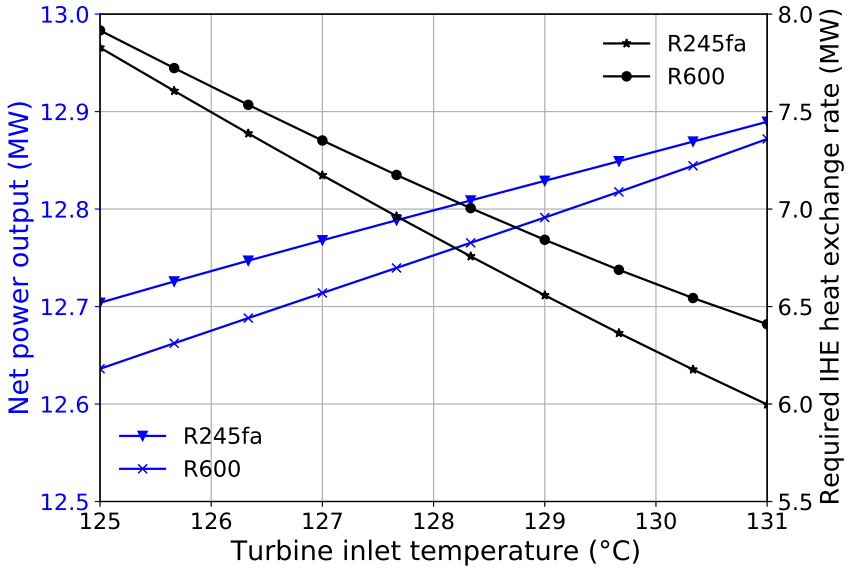

Figure 10: The net power output and the required minimum heat exchange rate of IHE for R245fa and R600 to keep the re-injection temperature at 70 °C.

As already been pointed out by Dai et al. [28], the installation of IHE only increases the thermal efficiency and net power output. For the plant designers, the third working fluid category (R245fa and R600) requires the IHE size to be dramatically increased, when the geothermal resources degrades. Hence, the potential reasonable choice from thermodynamic perspective is the fluid with the highest net power output from the other two categories. To make an enlightened decision in real-world projects for the working fluid type, the site-specific economic analysis has to be conducted on the basis of thermodynamic analysis.

6.2. Impact of geo-steam fraction on the working fluid selection

As stated in the Introduction section, geothermal steam contains more energy than the brine. Hence, the steam fraction largely affects the amount of input enthalpy, which also affects the working fluid selection. For example, with a low steam mass fraction of 5 %, it is clearly observed in Fig. 11 that

maximum peak points can be found in both the gross and net power output curves, which is different from the monotonic increasing trend observed in Fig. 4. With this characteristics of the working fluid, the optimal turbine inlet temperature and the corresponding IHE size can be easily obtained to achieve the maximum net power output, and satisfy the re-injection temperature limit at the same time. With a reduction in geothermal fluid enthalpy, R600 and R245fa can be used as the working fluid, and establishing a stable ORC plant. On the contrary, if the geothermal steam mass fraction is larger than 10 %, the working fluid with a higher critical state is preferred.

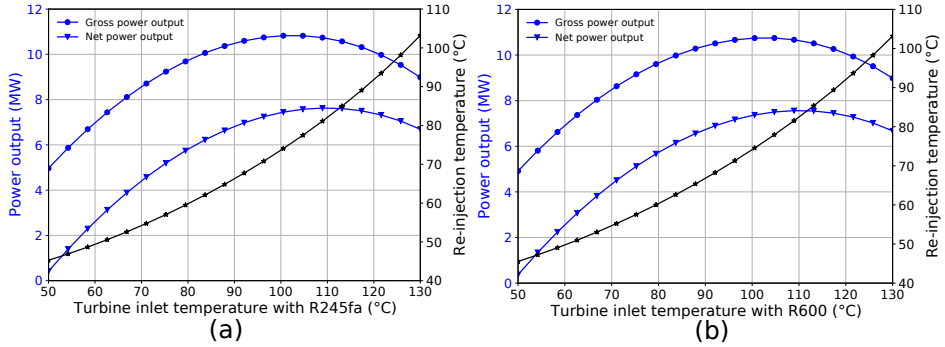

Figure 11: Gross, net power output and re-injection temperature for (a) the R245fa and (b) the R600 plant under different turbine inlet temperatures. The IHE is installed with the maximum size ($x_{\mathrm{IHE}} = 1$). The geothermal steam mass fraction is 5 %.

6.3. Re-injection temperature constrained by silica saturation

In comparison to existing literature on the topic of ORC based power plant, the design and optimization procedure presented in this work is specially tailored for the two-phase geothermal heat source. When designing such a plant, one particular constrain from the reservoir engineering consideration is the limitation on re-injection temperature. In many medium-to-high temperature geothermal fields, this temperature is constrained by the silica concentration in the geothermal fluids [55]. Since the solubility of silica decreases along with the dropping temperature, the saturation index of silica will gradually increase when the geo-fluid is passing through the evaporator and pre-heater. Empirically, the silica saturation index should be controlled less than 1.4 [56, 57], which means the temperature of re-injection geothermal brine cannot be set arbitrarily.

Since the silica concentrations from different geological sites varies greatly, it is important to have an uniform design and optimization process with silica constrain explicitly considered. As shown in the result section, the lower temperature limit will actually influence the choice of the working fluid, and the system's design specifications as well. In this study increasing the size of the IHE simultaneously benefits total power output and the re-injection temperature constraint with the air-cooling condenser. However, in comparison to the risk of clogging pipelines and re-injection wells, accepting the increase in investment cost even at reduction of output is the reasonable choice for most plant owners. In some high-temperature geothermal fields, silica concentration is so high that it cannot be simply controlled by adjusting the ORC design parameters. In that case, the plant has to be designed with geo-fluid acidification or adding silica dispersing chemicals [58, 59].

7. Conclusion and outlook

In this work, an ORC power plant has been designed for utilization of two-phase geothermal resources. Six potential working fluids are selected and the comparison in their performance has been conducted. From thermodynamic perspective, the gross power output and net power output have been optimized, respectively. The main findings are summarized as follows:

- A reproducible workflow for the investigation and optimization of thermodynamic properties of the two-phase geothermal ORC using different working fluids has been implemented.
- For the two-phase geothermal condition in this study, R245fa and R600 have no clear optimal turbine inlet temperatures, but having the optimal condensing temperature values, accounting for 31.11 °C for R245fa and 31.07 °C for R600. R600 has the highest gross power output of 17.55 MW, however, the turbine inlet temperature needs to be designed at its upper limit of 131 °C.
- Considering the ORC application on the hydro-thermal geothermal systems, the re-injection temperature needs to be elevated up to 70 °C by the IHE for the working fluid of R245ca, Isopentane, R600 and R245fa. The required IHE heat exchange rates of R245ca and Isopentane are 1.51 MW and 0.99 MW, which are lower than that with R600 (6.7 MW) and R245fa (6.0 MW). Meanwhile, the net power output can be increased by adding an IHE in ORC system as well because of the reduced thermal load on condenser.

- In order to establish a stable power plant, R245ca is found to be the best working fluid choice for the maximum net power output in Tibet geothermal condition, reaching at 11.82 MW with the maximum IHE heat exchange rate of 8.83 MW. For those two-phase geothermal sources with low steam mass fraction, the working fluid with low critical state is preferred.

The feasibility of electricity generation by different geothermal exploitation systems is not only decided by the plant technology, but also by the geothermal reservoir response. Therefore, the ORC power plant model in this work will be coupled with the geothermal reservoir model constructed in OpenGeoSys (OGS) software [60] in the future. Both the open-loop [61, 62] and closed-loop [63, 64] geothermal exploitation systems can be simulated with the OGS software. In addition, thermo-economic investigation can also be carried out on top of the thermodynamic design of the ORC plant, providing more straight-forward design comparison to the plant owners.

CRediT authorship contribution statement

Chaofan Chen and Francesco Witte are equal contributors to this work. **Chaofan Chen:** Conceptualization, Investigation, Formal analysis, Writing - Original Draft. **Francesco Witte:** Investigation, Methodology, Software, Data Curation, Formal analysis, Writing - Original Draft. **Ilja Tuschy:** Conceptualization, Investigation, Supervision, Writing - Review & Editing. **Olaf Kolditz:** Resources, Supervision. **Haibing Shao:** Conceptualization, Writing - Review & Editing, Supervision.

Declaration of competing interest

The authors declare that they have no competing financial interests or personal relationships that could have appeared to influence the work reported in this paper.

Acknowledgments

We thank the China Scholarship Council (CSC) for funding Chaofan Chen's PhD study in Germany. Funding for the project was provided also by the German Federal Ministry of Economic Affairs and Energy under Grant No. 03ET6122B ("ANGUS II: Impacts of the use of the geological subsurface for thermal, electrical or material energy storage in the context of

the transition to renewable energy sources – Integration of subsurface storage technologies into the energy system transformation using the example of Schleswig-Holstein as a model area") and is gratefully acknowledged.

Availability of data and materials

For the details of the calculation procedure, interested readers may refer to the Python scripts found at [37]. The source code and corresponding benchmarks of the TESPy software package are available on its official website: `https://tespy.readthedocs.io`. The TESPy version used in this publication is version 0.4.3.005 [65].

References

[1] B. F. Tchanche, G. Lambrinos, A. Frangoudakis, G. Papadakis, Low-grade heat conversion into power using organic rankine cycles–a review of various applications, Renewable and Sustainable Energy Reviews 15 (2011) 3963–79.

[2] Z. Shengjun, W. Huaixin, G. Tao, Performance comparison and parametric optimization of subcritical organic rankine cycle (orc) and transcritical power cycle system for low-temperature geothermal power generation, Applied energy 88 (2011) 2740–54.

[3] S. J. Zarrouk, H. Moon, Efficiency of geothermal power plants: A worldwide review, Geothermics 51 (2014) 142–53.

[4] U. Desideri, G. Bidini, Study of possible optimisation criteria for geothermal power plants, Energy Conversion and Management 38 (1997) 1681–91.

[5] P. Garg, P. Kumar, K. Srinivasan, P. Dutta, Evaluation of isopentane, r-245fa and their mixtures as working fluids for organic rankine cycles, Applied Thermal Engineering 51 (2013) 292–300.

[6] D. Hu, S. Li, Y. Zheng, J. Wang, Y. Dai, Preliminary design and off-design performance analysis of an organic rankine cycle for geothermal sources, Energy Conversion and Management 96 (2015) 175–87.

[7] C. Alimonti, P. Conti, E. Soldo, A comprehensive exergy evaluation of a deep borehole heat exchanger coupled with a orc plant: The case study of campi flegrei, Energy 189 (2019) 116100.

[8] R. S. El-Emam, I. Dincer, Exergy and exergoeconomic analyses and optimization of geothermal organic rankine cycle, Applied Thermal Engineering 59 (2013) 435–44.

[9] D. Fiaschi, A. Lifshitz, G. Manfrida, D. Tempesti, An innovative orc power plant layout for heat and power generation from medium-to low-temperature geothermal resources, Energy conversion and management 88 (2014) 883–93.

[10] E. Kaya, S. J. Zarrouk, M. J. O'Sullivan, Reinjection in geothermal fields: a review of worldwide experience, Renewable and sustainable energy reviews 15 (2011) 47–68.

[11] Z. Kamila, E. Kaya, S. J. Zarrouk, Reinjection in geothermal fields: An updated worldwide review 2020, Geothermics 89 (2021) 101970.

[12] E. Jolie, S. Scott, J. Faulds, I. Chambefort, G. Axelsson, L. C. Gutierrez-Negrin, S. Regenspurg, M. Ziegler, B. Ayling, A. Richter, et al., Geological controls on geothermal resources for power generation, Nature Reviews Earth & Environment (2021) 1–16.

[13] Y. Wang, C. Li, J. Zhao, B. Wu, Y. Du, J. Zhang, Y. Zhu, The above-ground strategies to approach the goal of geothermal power generation in china: State of art and future researches, Renewable and Sustainable Energy Reviews (2020) 110557.

[14] M. Grassiani, Siliceous scaling aspects of geothermal power generation using binary cycle heat recovery, Transactions-Geothermal Resources Council (2000) 475–8.

[15] A. Franco, M. Villani, Optimal design of binary cycle power plants for water-dominated, medium-temperature geothermal fields, Geothermics 38 (2009) 379–91.

[16] J. Sun, Q. Liu, Y. Duan, Effects of evaporator pinch point temperature difference on thermo-economic performance of geothermal organic rankine cycle systems, Geothermics 75 (2018) 249–58.

[17] A. Franco, M. Vaccaro, An integrated "reservoir-plant" strategy for a sustainable and efficient use of geothermal resources, Energy 37 (2012) 299–310.

[18] H. M. Hettiarachchi, M. Golubovic, W. M. Worek, Y. Ikegami, Optimum design criteria for an organic rankine cycle using low-temperature geothermal heat sources, Energy 32 (2007) 1698–706.

[19] A. Toffolo, A. Lazzaretto, G. Manente, M. Paci, A multi-criteria approach for the optimal selection of working fluid and design parameters in organic rankine cycle systems, Applied Energy 121 (2014) 219–32.

[20] W. Su, Y. Hwang, S. Deng, L. Zhao, X. Nie, Y. Zhang, et al., Error analysis of orc performance calculation based on the helmholtz equation with different binary interaction parameters of mixture, Energy 166 (2019) 414–25.

[21] X. Wang, X. Liu, C. Zhang, Parametric optimization and range analysis of organic rankine cycle for binary-cycle geothermal plant, Energy conversion and management 80 (2014) 256–65.

[22] Q. Liu, A. Shen, Y. Duan, Parametric optimization and performance analyses of geothermal organic rankine cycles using r600a/r601a mixtures as working fluids, Applied Energy 148 (2015) 410–20.

[23] M. Jankowski, A. Borsukiewicz, Multi-objective approach for determination of optimal operating parameters in low-temperature orc power plant, Energy Conversion and Management 200 (2019) 112075.

[24] J. Vivian, G. Manente, A. Lazzaretto, A general framework to select working fluid and configuration of orcs for low-to-medium temperature heat sources, Applied Energy 156 (2015) 727–46.

[25] O. Aboelwafa, S.-E. K. Fateen, A. Soliman, I. M. Ismail, A review on solar rankine cycles: Working fluids, applications, and cycle modifications, Renewable and Sustainable Energy Reviews 82 (2018) 868–85.

[26] W. Xu, S. Deng, W. Su, Y. Zhang, L. Zhao, Z. Yu, How to approach carnot cycle via zeotropic working fluid: Research methodology and case study, Energy 144 (2018) 576–86.

[27] B. Saleh, G. Koglbauer, M. Wendland, J. Fischer, Working fluids for low-temperature organic rankine cycles, Energy 32 (2007) 1210–21.

[28] Y. Dai, J. Wang, L. Gao, Parametric optimization and comparative study of organic rankine cycle (orc) for low grade waste heat recovery, Energy Conversion and Management 50 (2009) 576–82.

[29] S. M. Bina, S. Jalilinasrabady, H. Fujii, Energy, economic and environmental (3e) aspects of internal heat exchanger for orc geothermal power plants, Energy 140 (2017) 1096–106.

[30] M. Kahraman, A. B. Olcay, E. Sorgüven, Thermodynamic and thermoeconomic analysis of a 21 mw binary type air-cooled geothermal power plant and determination of the effect of ambient temperature variation on the plant performance, Energy Conversion and Management 192 (2019) 308–20.

[31] Z. Wang, N. Zhou, J. Guo, X. Wang, Fluid selection and parametric optimization of organic rankine cycle using low temperature waste heat, Energy 40 (2012) 107–15.

[32] I. H. Aljundi, Effect of dry hydrocarbons and critical point temperature on the efficiencies of organic rankine cycle, Renewable Energy 36 (2011) 1196–202.

[33] C. He, C. Liu, M. Zhou, H. Xie, X. Xu, S. Wu, Y. Li, A new selection principle of working fluids for subcritical organic rankine cycle coupling with different heat sources, Energy 68 (2014) 283–91.

[34] I. H. Bell, J. Wronski, S. Quoilin, V. Lemort, Pure and pseudo-pure fluid thermophysical property evaluation and the open-source thermophysical property library coolprop, Industrial & Engineering Chemistry Research 53 (2014) 2498–508. doi:10.1021/ie4033999.

[35] F. Witte, I. Tuschy, TESPy: Thermal Engineering Systems in Python, Journal of Open Source Software 5 (2020) 2178. doi:10.21105/joss.02178.

[36] F. Witte, J. Meier, M. Hofmann, I. Tuschy, G. Tsatsaronis, Thermal Engineering Systems in Python (TESPy): The implementation and validation of a generic exergy analysis, Submitted to Energy (2022). Under review.

[37] F. Witte, C. Chen, Two-phase Geothermal Source ORC Power Plant, v1.1, 2021. doi:10.5281/zenodo.5918217.

[38] F. Witte, Thermal Engineering Systems in Python, https://tespy.readthedocs.io/en/main/, 2018. Accessed: 2022-01-04.

[39] T. F. Edgar, D. M. Himmelblau, Optimization of Chemical Processes, McGraw-Hill, 1988.

[40] A. Ravindran, K. M. Ragsdell, G. V. Reklaitis, Engineering Optimization, John Wiley & Sons, Inc., 2006. doi:10.1002/9780470117811.

[41] J. Kiefer, Sequential minimax search for a maximum, Proceedings of the American Mathematical Society 4 (1953) 502–5. doi:10.1090/s0002-9939-1953-0055639-3.

[42] F. Biscani, D. Izzo, A parallel global multiobjective framework for optimization: pagmo, Journal of Open Source Software 5 (2020) 2338. doi:10.21105/joss.02338.

[43] M. Schlüter, J. A. Egea, J. R. Banga, Extended ant colony optimization for non-convex mixed integer nonlinear programming, Computers & Operations Research 36 (2009) 2217–29. doi:10.1016/j.cor.2008.08.015.

[44] M. Mahdavi, M. Fesanghary, E. Damangir, An improved harmony search algorithm for solving optimization problems, Applied Mathematics and Computation 188 (2007) 1567–79. doi:10.1016/j.amc.2006.11.033.

[45] J. Bao, L. Zhao, A review of working fluid and expander selections for organic rankine cycle, Renewable and sustainable energy reviews 24 (2013) 325–42.

[46] T. F. Yee, I. E. Grossmann, Simultaneous optimization models for heat integration—ii. heat exchanger network synthesis, Computers & Chemical Engineering 14 (1990) 1165–84.

[47] C. A. Frangopoulos, Comparison of thermoeconomic and thermodynamic optimal design of a combined-cycle plant, Proceedings of Analysis of Thermal and Energy Systems (1991) 3–6.

[48] A. Bejan, G. Tsatsaronis, M. Moran, Thermal Design and Optimization, Wiley, 1996.

[49] P. Roosen, S. Uhlenbruck, K. Lucas, Pareto optimization of a combined cycle power system as a decision support tool for trading off investment vs. operating costs, International Journal of Thermal Sciences 42 (2003) 553–60. doi:10.1016/s1290-0729(03)00021-8.

[50] J. Silveira, C. Tuna, Thermoeconomic analysis method for optimization of combined heat and power systems. part i, Progress in energy and Combustion Science 29 (2003) 479–85.

[51] A. Valero, M. A. Lozano, L. Serra, G. Tsatsaronis, J. Pisa, C. Frangopoulos, M. R. von Spakovsky, Cgam problem: definition and conventional solution, Energy 19 (1994) 279–86.

[52] V. Stefansson, Geothermal reinjection experience, Geothermics 26 (1997) 99–139.

[53] E. K. Mroczek, S. P. White, D. J. Graham, Deposition of amorphous silica in porous packed beds—predicting the lifetime of reinjection aquifers, Geothermics 29 (2000) 737–57.

[54] T. Xu, Y. Ontoy, P. Molling, N. Spycher, M. Parini, K. Pruess, Reactive transport modeling of injection well scaling and acidizing at tiwi field, philippines, Geothermics 33 (2004) 477–91.

[55] S. J. Zarrouk, B. C. Woodhurst, C. Morris, Silica scaling in geothermal heat exchangers and its impact on pressure drop and performance: Wairakei binary plant, new zealand, Geothermics 51 (2014) 445–59.

[56] L. B. Villaseñor, A. A. Calibugan, Silica scaling in tiwi–current solutions, in: International Workshop on Mineral Scaling. Manila, Philippines, 2011.

[57] Y. Li, Z. Pang, I. M. Galeczka, Quantitative assessment of calcite scaling of a high temperature geothermal well in the kangding geothermal field of eastern himalayan syntax, Geothermics 87 (2020) 101844.

[58] D. L. Gallup, E. Barcelon, Investigations of organic inhibitors for silica scale control from geothermal brines–ii, Geothermics 34 (2005) 756–71.

[59] A. Kioka, M. Nakagawa, Theoretical and experimental perspectives in utilizing nanobubbles as inhibitors of corrosion and scale in geothermal power plant, Renewable and Sustainable Energy Reviews 149 (2021) 111373.

[60] O. Kolditz, S. Bauer, L. Bilke, N. Böttcher, J.-O. Delfs, T. Fischer, U. J. Görke, T. Kalbacher, G. Kosakowski, C. McDermott, et al., Opengeosys: an open-source initiative for numerical simulation of thermo-hydro-mechanical/chemical (thm/c) processes in porous media, Environmental Earth Sciences 67 (2012) 589–99.

[61] G. Blöcher, M. Cacace, T. Reinsch, N. Watanabe, Evaluation of three exploitation concepts for a deep geothermal system in the north german basin, Computers & Geosciences 82 (2015) 120–9.

[62] N. Watanabe, G. Blöcher, M. Cacace, S. Held, T. Kohl, Geoenergy Modeling III: Enhanced Geothermal Systems, Springer, 2016.

[63] C. Chen, H. Shao, D. Naumov, Y. Kong, K. Tu, O. Kolditz, Numerical investigation on the performance, sustainability, and efficiency of the deep borehole heat exchanger system for building heating, Geothermal Energy 7 (2019) 1–26.

[64] C. Chen, W. Cai, D. Naumov, K. Tu, H. Zhou, Y. Zhang, O. Kolditz, H. Shao, Numerical investigation on the capacity and efficiency of a deep enhanced u-tube borehole heat exchanger system for building heating, Renewable Energy 169 (2021) 557–72.

[65] F. Witte, TESPy: Thermal Engineering Systems in Python, v0.4.3.005, 2021. doi:10.5281/zenodo.4769063.